Experimental Evidence on Inward Momentum Pinch on JET and Comparison with Theory and Modelling

T. Tala[1], J. Ferreira[2], P. Mantica[3], A.G. Peeters[4], G. Tardini[5], P.C. de Vries[6], K.-D. Zastrow[6], M. Brix[6], G. Corrigan[6], C. Giroud[6], I. Jenkins[6], V. Naulin[7], D. Strintzi[8], T. Versloot[9] and JET-EFDA contributors*

JET-EFDA, Culham Science Centre, Abingdon, OX14 3DB, United Kingdom
[1]Association EURATOM-Tekes, VTT, P.O. Box 1000, FIN-02044 VTT, Finland
[2]Associação EURATOM/IST, Centro de Fusão Nuclear, 1049-001 Lisbon, Portugal
[3]Istituto di Fisica del Plasma CNR-EURATOM, via Cozzi 53, 20125 Milano, Italy
[4]Center for Fusion, Space and Astrophysics, Department of Physics, Univ. of Warwick, United Kingdom
[5]Max-Planc-Iinstitut für Plasmaphysik, EURATOM-Assoziation, Garching, Germany
[6]EURATOM/UKAEA Fusion Association, Culham Science Centre, United Kingdom
[7]Association Euratom-Risø-DTU, Denmark
[8]National Technical University of Athens, Euratom Association, GR-15773 Athens, Greece
[9]FOM Instituut for Plasmafysica Rijnhuizen, Association EURATOM-FOM, Nieuwegein, The Netherlands
*See Appendix of F. Romanelli *et al.*, Fusion Energy Conference 2008 (Proc. 22nd Int. Conf. Geneva 2008), IAEA Vienna (2008)

Email: tuomas.tala@vtt.fi

Abstract: Experiments have been carried out on the Joint European Torus (JET) tokamak to determine the diffusive and convective momentum transport. Torque, injected by neutral beams, was modulated to create a periodic perturbation in the toroidal rotation velocity. Novel transport analysis shows the magnitude and profile shape of the momentum diffusivity is similar to those of the ion heat diffusivity. A significant inward momentum pinch, up to 20 m/s, has been found. Both results are consistent with recent developments in momentum transport theory and gyro-kinetic simulations. This evidence is complemented in plasmas with internal transport barriers.

1. Introduction

Plasma rotation and momentum transport in tokamaks are currently a very active research area. It is well-known that sheared rotation can lead to quenching of turbulence and a subsequent improvement in confinement [1,2]. Toroidal rotation also increases stability against pressure limiting resistive wall modes [3]. Still, transport of toroidal momentum is less understood than heat or particle transport. Extrapolating reliably the toroidal rotation, in magnitude and profile shape to future tokamaks, such as ITER, remains a challenge, as neither momentum transport nor sources are known precisely.

One way to increase the understanding of momentum transport is to compare it with heat transport as for the conditions where the Ion Temperature Gradient (ITG) instability is dominantly driving anomalous transport, both transport channels are predicted to be similar [4,5]. The momentum diffusivity χ_ϕ and pinch velocity v_{pinch} (negative sign denotes inwards) are related to the toroidal velocity v_ϕ, its gradient ∇v_ϕ and the momentum flux Γ_ϕ, assuming the absence of a significant particle flux, as follows:

$$\Gamma_\phi \sim -\chi_\phi \nabla(v_\phi n) + v_{pinch} v_\phi n = -\chi_{\phi,eff} \nabla(v_\phi n), \quad (1)$$

where n is the ion density. It is always possible to combine the diffusive and convective part of the momentum flux into an effective momentum diffusivity $\chi_{\phi,eff}$. This quantity can be easily determined from steady-state transport analysis once the sources are known while the determination of χ_ϕ and v_{pinch} separately requires more sophisticated experiments.

A rotation database covering more than 600 JET discharges shows that the effective Prandtl number, $P_{r,eff} = \chi_{\phi,eff}/\chi_{i,eff} \approx 0.1$–$0.4$ is substantially below one in the JET core plasma [6,7], shown in figure 1. Somewhat larger values for $P_{r,eff}$ have been reported on other tokamaks [8,9]. The low $P_{r,eff}$ is in apparent contradiction with ITG based theories and gyro-kinetic calculations, which report 'purely diffusive' Prandtl number $P_r = \chi_\phi/\chi_i \approx 1$, with only weak dependencies on plasma parameters, like q, magnetic shear or density and temperature gradient [5,10]. Recent developments in theory predict a sizeable inward momentum pinch. This could resolve the discrepancy as the inward pinch results in $P_{r,eff}$ being smaller than P_r [11,12]. Until now experimental evidence for an inward evidence for an inward momentum pinch only been reported on the JT-60U tokamak [13]. In this paper in section 2, we present experimental evidence of a significant inward momentum pinch in JET, using torque modulation techniques. This evidence is complemented with observations in plasmas with Internal Transport Barriers (ITBs) showing different dynamic behaviour between ion temperature and toroidal velocity section 3.

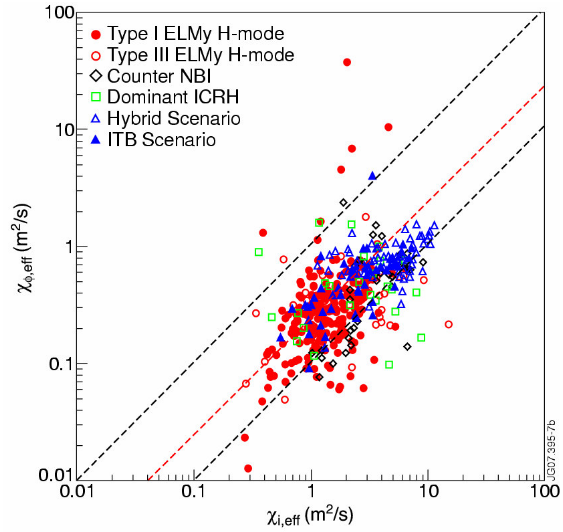

Figure 1.Effective momentum diffusivity versus effective ion heat diffusivity from JET momentum database.

2. NBI Modulation Experiments on JET

Studying heat transport by modulation of localised, electron or ion cyclotron resonance heating is a well established technique [14]. For momentum, the only significant torque source which can be modulated originates from the Neutral Beam Injection (NBI) system. Passing ions transfer toroidal angular momentum to the bulk plasma by collisions which is a slow process, whereas trapped ions transfer their momentum by $\mathbf{j} \times \mathbf{B}$ forces which is practically instantaneous ($\mathbf{j}$ denotes displacement current density due to finite banana orbit width and $\mathbf{B}$ magnetic field) [15].

2.2.1 Experimental Set-up

An experiment where the NBI power and torque were modulated at 6.25 Hz (NBI 80ms ON and 80 ms OFF) has been performed on JET. This modulation frequency is much lower than the 10ms time resolution of the Charge Exchange Recombination Spectroscopy (CXRS) diagnostic used to measure the toroidal rotation ω_ϕ and ion temperature T_i at 12 radial points [16,17]. The modulation took place between t=4s and t=13s, using 3 tangential beams for a total of about 5 MW of modulated power, the total NBI power then varying between 10 and 15 MW. Time traces of experimental toroidal angular rotation frequency ω_ϕ and calculated torque for 9 of the modulation cycles are illustrated in figure 2(b) and (c), showing a clear modulation in ω_ϕ.

To perform the cleanest possible toroidal rotation modulation and to avoid MHD modes, a *H*-mode plasma with type III ELMs, low collisionality and high q_{95} was chosen. Under these conditions, ITG is the dominant instability, making the coupling of momentum and ion heat transport, and thus the concept of the Prandtl number, unambiguous.

2.2.2 Calculation of the Torque Profiles

The NBI induced torque has been calculated with the NUBEAM code [18] inside the TRANSP transport code. No AE activity or any other MHD mode is observed that could re-distribute NBI driven fast ions and further have an impact on the calculated torque profiles from TRANSP.

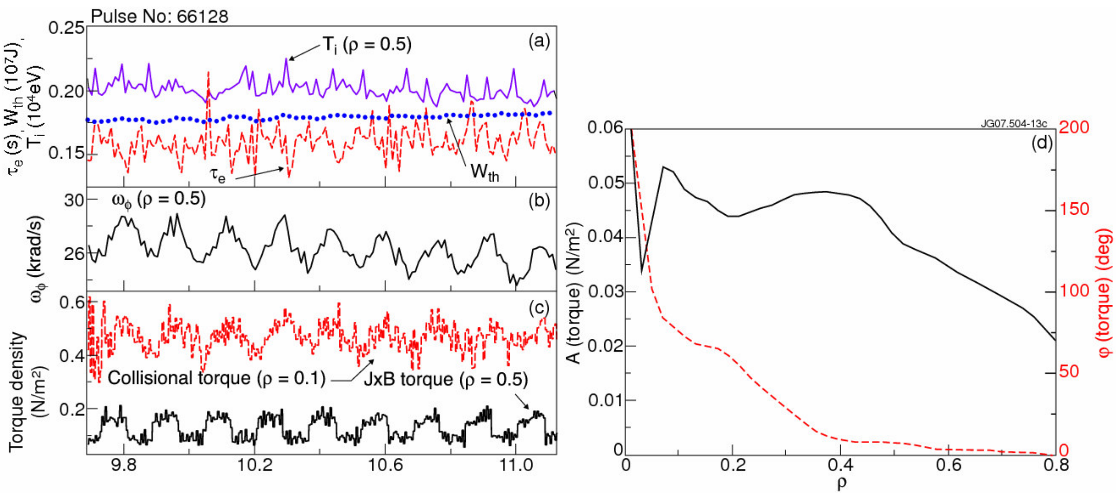

Figure 2. Time traces of (a) T_i, stored thermal energy W_{th} and confinement time τ_E, (b) toroidal angular frequency ω_ϕ, (c) two components of the torque density for JET pulse no. 66128. (d) Amplitude (solid black) and phase (dashed red) of the modulated calculated total torque.

In order to obtain a torque modulation signal far beyond noise, 160 000 particles have been used in the Monte-Carlo calculation of NBI torque. All phases are calculated with reference to the phase of the NBI power. The calculated amplitude and phase at 6.25Hz of the modulated torque density profiles over the same 9 modulation cycles are shown in figure 2(d) as a function of the normalised toroidal flux co-ordinate. Outside ρ>0.4 the torque is dominated by the $\mathbf{j} \times \mathbf{B}$ component and synchronous with the injected power while in the central part of the plasma, the collisional component dominates, resulting in a delay of about 50ms due to the slowing down time of the fast ionised beam particles. Very similar torque density profiles as those from TRANSP have been calculated with ASCOT orbit following Monte-Carlo code [19], showing the robustness of the NBI torque calculation. As the modulated torque is not radially localised, a simple determination of the momentum diffusivity and pinch directly from the spatial derivatives of the amplitude and phase of the modulated ω_ϕ is not viable. Therefore, time-dependent transport modelling of ω_ϕ is required.

The level of intrinsic rotation in Ohmic plasmas is typically only a few percent of the rotation in these experiments with relatively large NBI power and thus, we can ignore the torque source driving the intrinsic rotation. In addition, as the plasma thermal energy is not modulated with NBI (shown in figure 2(a)), the intrinsic rotation is not expected to be modulated either. Furthermore, other torque sources or sinks, such as torque due to fast ion losses originating from toroidal magnetic field ripple, ICRH driven rotation or plasma braking due to intrinsic error fields in these low β plasmas are negligible as compared with NBI driven torque.

2.2.3 The Analysis Method to Infer the Momentum Pinch and Diffusivity

The novel transport modelling methodology adopted in this study to determine the momentum diffusivity and pinch uses the following 3 steps: step 1, calculate $\chi_{i,eff}$; step 2, vary the P_r value and its radial profile to fit the simulated phase of the modulated rotation to the experimental phase profile, as the diffusivity is the main contributor to the phase while v_{pinch} playing only a minor role, as shown in ref. [20]; step 3, vary v_{pinch} to best fit also the simulated amplitude of the modulated toroidal rotation to the experimental data, simultaneously also matching the steady-state. In step 1 $\chi_{i,eff}$ is calculated from the measured T_i data and calculated power deposition profiles. Here, we assume that there is no ion heat pinch, a result supported also in recent T_i modulation experiments [21]. Step 2 leads to a rather precise identification of the acceptable range of P_r values, since P_r is the only unknown (the sources are taken from the NUBEAM calculations). This resolves the indeterminacy associated with the analysis of only the steady-state profile, as the latter can be reproduced by an unlimited number of possible combinations for χ_ϕ and v_{pinch} yielding the same $\chi_{\phi,eff}$. Once P_r is identified, step 3 allows us to identify v_{pinch} needed to reproduce the steady-state ω_ϕ and amplitude with the chosen P_r value. As a refinement, P_r, instead of being constant, can be chosen to have a radial profile, taken e.g. from gyro-kinetic simulations.

2.2.4 Experimental Results and Comparison with Theory

Figures 3–4 compare experimental data and simulations for ω_ϕ steady-state and modulated amplitude $A_{\omega,\phi}$ and phase $\varphi_{\omega,\phi}$. The experimental profiles have been mapped onto a moving equilibrium to eliminate the spurious modulation components due to modulated plasma position. For the simulations, the two most obvious options for χ_ϕ or P_r and v_{pinch} were adopted: (i) fix P_r=0.25 to yield $\chi_\phi = 0.25\chi_{i,eff}$ and v_{pinch}=0 or (ii) match the simulated and experimental phase by fitting P_r, using the profile shape from gyro-kinetic simulations with GKW [22] and then vary the v_{pinch} profile to additionally match the simulated and experimental amplitudes and steady-state. All simulations for ω_ϕ have been performed with the JETTO transport code. The transport equation for ω_ϕ is solved while q, T_i, T_e and n_e are frozen to their experimental values. The boundary conditions for steady-state ω_ϕ and the amplitudes $A_{\omega,\phi}$ and phases $\varphi_{\omega,\phi}$ of the modulated ω_ϕ are chosen to fit the experimental data at ρ=0.8. The transport simulations are carried out over the 9 modulation cycles shown in figure 2.

Both simulations (i) and (ii) predict the steady-state ω_ϕ within 10% accuracy in the region of interest, i.e. $0.2<\rho<0.8$, as seen in figure 3. Inside $\rho<0.2$, neo-classical transport starts to dominate ion heat transport, and the predictions are worse as the use of the ITG based P_r for calculating χ_ϕ is not appropriate.

Options (i) and (ii) differ, however, in reproducing the $A_{\omega,\phi}$ and $\varphi_{\omega,\phi}$ profiles as shown in figure 4. Case (i) with P_r = 0.25 and v_{pinch}= 0 clearly disagrees with the experiments. The simulated phase is too large, an indication of too low χ_ϕ, i.e. too low P_r used in the simulation. On the other hand, the simulated amplitude is too low towards the plasma centre, which could only be cured by lowering χ_ϕ further. This shows that the assumption v_{pinch}= 0 is not compatible with the experimental data. Case (ii) uses $P_r = \chi_\phi/\chi_i$~1 from GKW (figure 4(c)) and v_{pinch} varying radially between 0 and –25 m/s (figure 4(d)). This improves the agreement between the simulated and experimental amplitudes and phases dramatically. The $\chi_{i,eff}$ used as χ_i (heat pinch assumed to be zero) to multiply P_r, is also shown in figure 4(d). This v_{pinch} profile reproduces best the experimental amplitude and phase profiles, together with an acceptable reproduction of the steady-state toroidal rotation profile. v_{pinch} is roughly proportional to χ_ϕ, consistent with the predictions by the theory [11,12]. Uniform P_r=1.0 instead of using P_r from GKW and the same v_{pinch} results in almost as good agreement with experiment. Finally, while the P_r numbers from GKW used in the JETTO simulations are in excellent agreement with experiment, and also very similar to those calculated with GS2 [23], there is some discrepancy in the pinch numbers, defined as Rv_{pinch}/χ_ϕ. The pinch numbers from GKW are 2–4, depending on radius, whereas the experimental ones are in the range of 3–8.

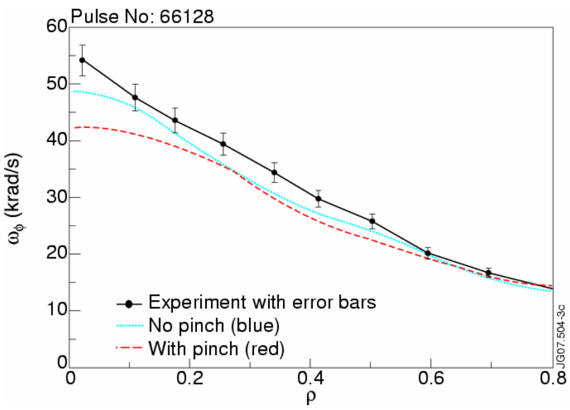

Figure 3. The simulated steady-state ω_ϕ with the two options (i) with P_r = 0.25 and v_{pinch}= 0 and frame (b) (dotted blue) and (ii) with $P_r \approx 1$ and v_{pinch} taken from figure (d) (dashed red) compared with the experimental ω_ϕ (solid black) with error bars.

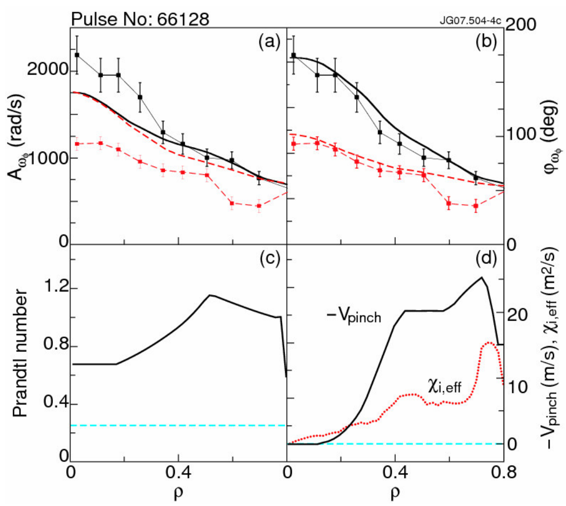

Figure 4. Comparison of the experimental amplitude (black solid with error bars) and phase (red dashed with error bars) and simulated amplitudes $A_{\omega,\phi}$ (black solid) and phases $\varphi_{\omega,\phi}$ (red dashed) of modulated ω_ϕ in frame (a) case (i) with P_r = 0.25 and v_{pinch}= 0 and frame (b) case (ii) with $P_r \approx 1$ and v_{pinch} taken from figure (d). (c) Prandtl numbers and (d) pinch velocity profiles used in cases (i) (blue dashed) and (ii) (black solid). Also shown the used $\chi_{i,eff}$ (red dotted) in frame (d).

More recently, the magnitude of the inward pinch and the Prandtl number has been confirmed on other JET discharges with similar plasma parameters. In these experiments, an asymmetric duty cycle (40ms ON, 80ms OFF) was used in order to obtain a perturbation also on the 2nd harmonic rotation. The instantaneous **j × B** torque is dominating the 1st harmonic everywhere outside 0.2 and 2nd harmonic consists almost solely of **j × B** torque as shown in figure 5(a) for JET discharge no. 73701. Figures 5(b) and 5(c) show the need to have an inward pinch in order to reproduce the amplitude and phase of the modulated toroidal rotation exactly in the same way shown in figure 4, i.e. the case with the low Prandtl number and without the pinch (figure 5(b)) has far too high predicted phase values while the case with the high Prandtl number and pinch (figure 5(c)) has the phase values much closer to the those of the experiments. The same conclusion can be drawn from the 2nd harmonic data.

2.2.5 Sensitivity Analysis of the Momentum Pinch and Diffusivity

A sensitivity analysis shows that 20–30% variability in P_r and v_{pinch} is compatible with experimental data, while outside this range the simulated phase and amplitude deviate unacceptably from the experimental values. The TRANSP torque calculations have been found very robust with respect to variations in plasma parameters.

One complicating factor requiring a careful assessment is that the ion and electron temperatures are also modulated with peak amplitudes around 70eV, i.e. a perturbation of just below 1% to be compared with the amplitude of the ω_ϕ modulation being around 4%. A time variation of T_i and/or its gradient length induces a time variation in the ITG driven transport, causing an oscillation in χ_i. This leads to an oscillation in χ_ϕ, yielding an extra contribution to $A_{\omega,\phi}$ and $\varphi_{\omega,\phi}$ and possibly modifying the determined P_r and v_{pinch}. To estimate the impact of such T_i modulation on the determined P_r and v_{pinch}, a time-dependent χ_i using an ion heat transport model based on the critical gradient length concept [24] and with the typical ion heat transport parameters found in JET ion heat transport studies [21,25], has been used to model the modulated T_i and the associated time variation of χ_i and χ_ϕ. Owing to the small amplitude of the T_i modulation (the amplitude of the time-dependent χ_i is 1-2% in the centre and decreases outside ρ>0.3), the effect on the values determined for P_r and v_{pinch} was insignificant. No modulation was experimentally observed for n_e or q.

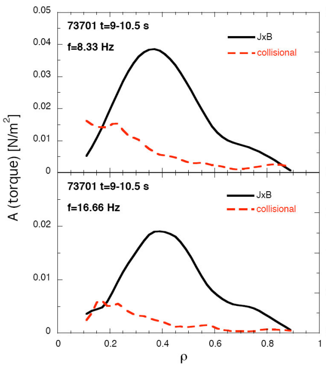

Figure 5(a). Different components of the modulated torque for JET shot no. 73701 for 1st harmonic (upper frame) and 2nd harmonic (lower frame).

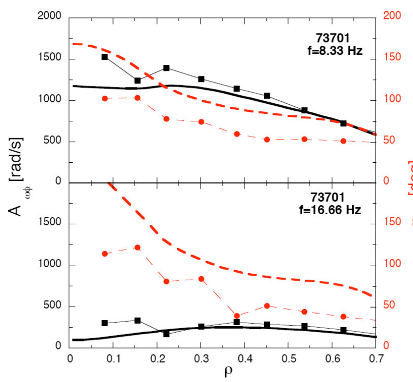

Figure 5(b). Experimental amplitude (black solid with squares) and phase (red dashed with squares) and simulated amplitudes $A_{\omega,\phi}$ (black solid) and phases $\varphi_{\omega,\phi}$ (red dashed) of modulated ω_ϕ with P_r = 0.25 and v_{pinch}= 0 for 1st harmonic (upper frame) and 2nd harmonic (lower frame).

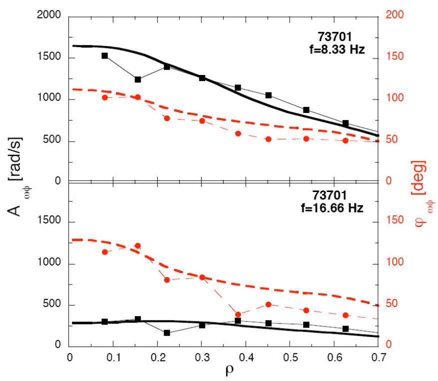

Figure 5(c). Experimental amplitude (black solid with squares) and phase (red dashed with squares) and simulated amplitudes $A_{\omega,\phi}$ (black solid) and phases $\varphi_{\omega,\phi}$ (red dashed) of modulated ω_ϕ with with $P_r \approx 1$ and v_{pinch} as in figure 4(d) for 1st harmonic (upper frame) and 2nd harmonic (lower frame).

3. Observation of Momentum Pinch in Plasmas with an ITB

Further, additional evidence of the existence of inward momentum pinch on JET comes from a plasma with an ITB. It has been reported that the footpoint of the ITB coincides between all transport channels (T_i, T_e, n_e, ω_ϕ) and that the radial expansion of the ITB occurs simultaneously for all channels [26]. The present experimental observation, however, illustrates that the footpoint of the ITB seems to be located at a slightly larger radius in T_i than in ω_ϕ as the ITB moves radially outwards. In figure 6, the T_i barrier is located within the CXRS channel (marked as horizontal lines in frame (d)) centred at r/a=0.48 whereas the ω_ϕ barrier is located one CXRS channel more inwards, i.e. centred at r/a=0.41 at t=5.29–5.31s. This can be seen clearly in frames (c) and (d) where there is virtually no difference in $\Delta\omega_\phi$ (between blue (dotted) and magenta (plusses) curves) while there is a significant difference in ΔT_i at r/a=0.48.

At t=5.35s, the ω_ϕ barrier also appears at r/a=0.48 (black stars). The ITB moves steadily outwards, following the outward movement of the q_{min} surface, the footpoint reaching a radius r/a=0.65 until the ITB collapses at t=5.95s. During its radial outward movement, the ITB passes two other CXRS channels at r/a=0.58 at t=5.34s and r/a=0.66 at t=5.77s. Both times, the ITB is seen first in T_i and after a few tens of milliseconds in ω_ϕ, indicating that the footpoint of the ITB is indeed located at a more outward radius for T_i than for ω_ϕ. The actual distance between the footpoints of the ITB in T_i and ω_ϕ is, however, much less than the distance between two CXRS channels. This phenomenon is only seen during the fast expansion of the ITB and never with stationary or slowly moving ITBs.

In order to understand this observation, two hypotheses have been tested: (1) in the absence of v_{pinch}, ω_ϕ could respond more slowly than T_i to the turbulence suppression within the ITB as $\chi_{i,eff}$ is larger than χ_ϕ=$\chi_{\phi,eff}$, i.e. $P_{r,eff}$ =0.3 for this discharge and (2) an inward toroidal momentum pinch causes an apparent delay to the outward movement of the ITB in the ω_ϕ channel, combined with higher χ_ϕ yielding P_r≈1. To study these hypotheses, predictive transport simulations for T_i and ω_ϕ have been performed, with initial conditions for T_i and ω_ϕ taken from pulse no. 69670. After reaching steady-state, the radial outward movement of the ITB in the ion heat transport channel is simulated by moving the low χ_i region outwards with time. For momentum transport, the two options (1) and (2) are applied. In the simulation with $P_{r,eff}$=0.3 and v_{pinch}=0, T_i and ω_ϕ react to the change of χ_i in the same way, resulting in the footpoint of the ITB being exactly the same. In case (2), the v_{pinch} profile is assumed to be proportional to χ_i and normalised to the value consistent with the value found in the NBI modulation experiment (v_{pinch}≈−15 m/s outside the ITB). This simulation shows that ω_ϕ responds more slowly to the radial outward movement of the ITB than T_i at the location of the ITB, as seen in figure 7. This is consistent with the CXRS measurements showing the rise of T_i just before the rise of ω_ϕ when the ITB passes the CXRS channel during its radial outward movement. It is to be noted that simulation (2) is sensitive to the v_{pinch} radial profile, which, in the absence of NBI modulation, cannot be determined. Here, we have assumed that inside the ITB, the magnitude of v_{pinch} is linked to the level of turbulence suppression, i.e. v_{pinch}~ χ_i.

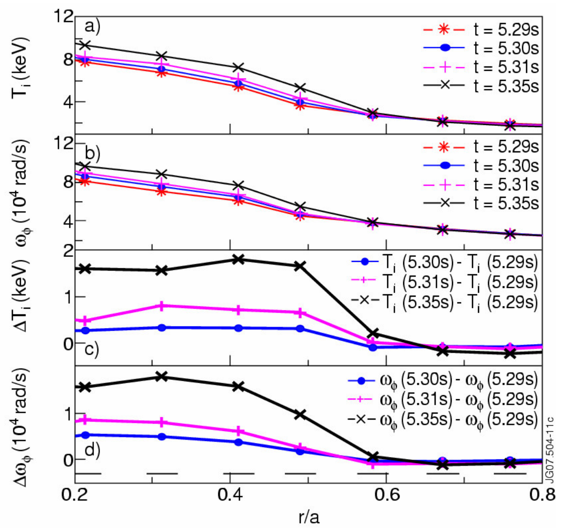

Figure 6. (a) T_i, (b) ω_ϕ, (c) ΔT_i and (d) $\Delta\omega_\phi$ profiles for JET pulse 69670 during the radial expansion of the ITB. The horizontal lines shown in frame (d) indicate the radial widths of the CXRS measurements points.

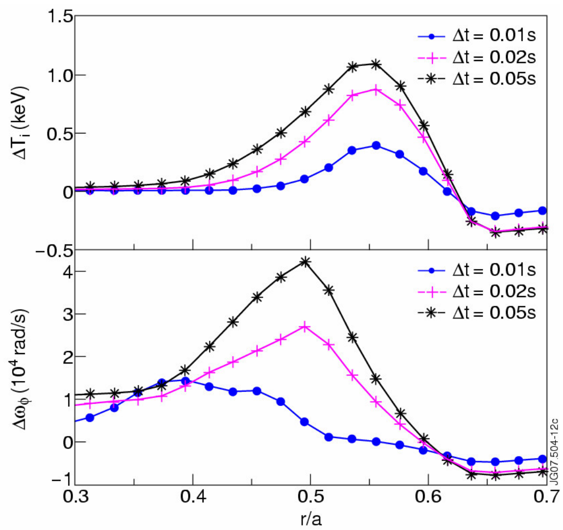

Figure 7. As in figure 6, but for simulated (a) ΔT_i and (b) $\Delta\omega_\phi$ profiles with a model of v_{pinch}≈−15m/s and P_r=1.0.

4. Summary

In summary, consistent evidence for a significant inward momentum pinch has been found in JET. This can explain why the observed small ratio of the effective momentum diffusivity to the ion heat diffusivity ($\chi_{\phi,\mathrm{eff}}/\chi_{i,\mathrm{eff}} \approx 0.1$–$0.4$) in the JET core plasma. The experimental values for the Prandtl numbers ($P_r \approx 0.7$-1) are in good agreement with those predicted by Gyrokinetic codes. The observed value of the pinch number Rv_{pinch}/χ is roughly a factor of two higher than those predicted by theory. The existence of the significantly large inward pinch velocity may have important implications on the predictions for the toroidal velocity profile in ITER. In particular, a centrally peaked toroidal velocity profile may still result even in the absence of any external core momentum source. It still remains to be assessed if the parametric dependences of such a pinch term are such that a sizeable convective component will be present in ITER plasmas.

Acknowledgements: This work, supported by the European Communities under the contract of Association between EURATOM and Tekes, was carried out within the framework of the European Fusion Development. The views and opinions expressed herein do not necessarily reflect those of the European Commission.

[1] Biglari H. *et al.*, Phys. Fluids B **2**, 1 (1990).
[2] Burrell K.H., Phys. Plasmas **4**, 1499 (1997).
[3] Garofalo A.M. *et al.*, Nucl. Fusion **41**, 1171 (2001).
[4] Mattor N. *et al.*, Phys. Fluids **31**, 1180 (1988).
[5] Peeters A.G. *et al.*, Phys. Plasmas **12**, 072515 (2005).
[6] P.C. de Vries *et al.*, Nucl. Fusion **48** (2008) 065006.
[7] Tala T. *et al.*, Plasma Phys. Control. Fusion **49**, B291 (2007).
[8] Nishijima D. *et al.*, Plasma Phys. Control. Fusion **47**, 89 (2005).
[9] de Grassie J.S. *et al.*, Nucl. Fusion **43**, 142 (2003).
[10] Strintzi D. *et al.*, Phys. Plasmas **15,** 044502 (2008).
[11] Peeters A.G. *et al.*, Phys. Rev. Lett. **98**, 265003 (2007).
[12] Hahm T.S. *et al.*, Phys. of Plasmas **14**, 072302 (2007).
[13] Yoshida M. *et al.*, Nucl. Fusion **47**, 856 (2007).
[14] Lopez Carzodo N. J., Plasma Phys. Control. Fusion **37**, 799 (1995).
[15] Zastrow K.-D. *et al.*, Nuclear Fusion **38**, 257 (1998).
[16] Negus C.R. *et al.*, Rev. Sci. Instr. **77**, 10F102 (2006).
[17] Giroud C. *et al.* Rev. Scientific Instruments, **79** 1 (2008).
[18] Pankin A. *et al.*, Computer Physics Communications **159**, 157 (2004).
[19] Heikkinen J.A. *et al.*, Journal of Computational Physics **173**, 527 (2001).
[20] P.Mantica *et al.*, Nucl. Fusion **32,** 2203 (1992).
[21] Ryter F. *et al.*, this conference, paper EX/P5-19 (2008).
[22] Peeters A.G. *et al.*, Phys. Plasmas **11**, 3748 (2004).
[23] Kotschenreuther M. *et al.*, Computational Phys. Communication **88**, 128 (1995).
[24] Garbet X. *et al.*, Plasma Phys. Control. Fusion **46**, 1351 (2004).
[25] P.Mantica *et al.*, this conference, paper EX/2-4 (2008).
[26] Challis C.D *et al.*, Plasma Phys. Control. Fusion **44**, 1031 (2002).